Picosecond laser-induced breakdown at 5321 and 3547 Å: Observation of frequency-dependent behavior*

W. Lee Smith,† J. H. Bechtel,‡ and N. Bloembergen
Gordon McKay Laboratory, Harvard University, Cambridge, Massachusetts 02138
(Received 27 October 1976)

Laser-induced dielectric breakdown at 5321 Å has been investigated in six materials: KH_2PO_4, fused SiO_2, NaCl, CaF_2, NaF, and LiF. The laser pulses were nominally 21 psec in duration and were obtained by the frequency doubling of single 1.064-μm pulses from a mode-locked YAlG:Nd laser system. The frequency doubling was carried out in a temperature phase-matched CsH_2AsO_4 crystal, resulting in spatially smooth, reproducible, diffraction-limited, 5321-Å pulses. Strict attention is given to the complications introduced by self-focusing. The new thresholds for breakdown at 5321 Å are compared with thresholds measured previously at 1.064 μm with the same laser system. This comparison, as a function of material band gap $\mathcal{E}_G$, charts experimentally the transition of the character of bulk laser-induced breakdown as it becomes strongly frequency dependent. A frequency-dependent decrease in the threshold of ~30% is observed for KH_2PO_4, for which three 5321-Å photons exceed $\mathcal{E}_G$ in energy. Frequency-dependent threshold increases of up to 44%, varying smoothly with $\mathcal{E}_G$, are observed for the other materials. At 3547 Å five materials were studied: KH_2PO_4, SiO_2, CaF_2, NaF, and LiF. The uv picosecond pulses were obtained by mixing 1.064-μm and 5321-Å pulses in a KH_2PO_4 crystal. In spite of uncertainties introduced by walk-off distortion and self-focusing, upper and lower bounds on the breakdown threshold at 3547 Å in these materials are obtained. These results qualitatively confirm and extend the behavior found in the 5321-Å study. These observations are discussed with regard to models for the intrinsic processes involved in the breakdown, which are avalanche and multiphoton ionization.

I. INTRODUCTION

In this paper we present experimental results which characterize the transition of laser-induced dielectric breakdown from the familiar dc limit into the regime where both avalanche ionization frequency dependence and multiquantum effects are clearly observed. This study represents a systematic frequency extension of our previous 1.064-μm investigations of picosecond dielectric breakdown in transparent solids.[1-3]

Laser-induced breakdown was reported in the literature early in the 1960s. However, the earnest study of dc breakdown has taken place since the 1930s. Indeed, it has been pointed out[4] that the laboratory observation of dc breakdown in glass was reported as early as 1799 by A. Van Marum.[5] Van Marum's efforts at producing high voltages were limited by breakdown through the walls of his storage jars. Beginning in 1931, experimental progress in dc breakdown threshold measurement was achieved by von Hippel.[6] Theoretical developments by Fröhlich[7] beginning in 1937 and Seitz[8] in 1949 proposed and described avalanche ionization as the basic physical mechanism involved in the dc case. In 1971 Yablonovitch performed laser-induced breakdown experiments[9] at 10.6 μm in which the similarity of the threshold between the infrared and earlier dc data, both in the trend with material composition and in absolute magnitudes, was compelling. Avalanche ionization was established as the intrinsic process whereby an infrared laser pulse is able to induce breakdown in pure dielectric material. Further controlled laser experiments at[10] 1.06 μm again found breakdown threshold not significantly different from those at dc and 10.6 μm, either in trend or magnitude. At the still shorter ruby wavelength of 6943 Å, a systematic increase over previous thresholds was reported.[11] As will be discussed in a later section, the pattern of increase was unusual, however, and it now appears that the threshold increase in the low-band-gap materials may have been an artifact. Yet at least part of the large relative increase in the NaF threshold reported in that study was quite probably an observation of true behavior and therefore the first indication of frequency dependence in avalanche ionization breakdown processes. An increased resistance to surface damage in several materials at 6943 Å over that at 1.064 μm was also reported[12] in 1973. Because that investigation involved rather different experimental conditions (surface breakdown, irradiation of the same sample volume with many pulses) from the present work, we will not discuss it further.

At wavelengths shorter than 6943 Å several experiments have been performed to date.[13-18] However, in each of these experiments self-focusing was present and no attempt was made to extract the self-focusing influence in order to measure a breakdown threshold. At best, such

experiments yield a measure of the critical power for self-focusing. Further interpretive difficulties were caused by the use of multimode lasers, entire mode-locked pulse trains, or harmonic generation crystals allowing walk-off. Under such conditions reliable breakdown thresholds are rarely obtainable.

Thus, up to electromagnetic angular frequencies ω of almost 3×10^{15} Hz, the basic behavior of bulk dielectric breakdown has been observed to be quite similar to the behavior at zero hertz. The concise reasons for this steadfast behavior over such a remarkable frequency range are twofold: (i) The hot-electron collision time (τ_c) in dielectrics is very fast ($<10^{-15}$ sec). (ii) In experiments up to 6943 Å, the photon energies were not a sufficiently sizable fraction of the material band gap $\mathcal{E}_G$. In Fig. 1 we illustrate the schematic frequency dependence of the breakdown threshold E_B, as has been anticipated for some time.[19] The low-frequency, pure avalanche region (solid segment) is the range of investigation prior to this study. As discussed elsewhere,[9] the relation

$$E_B(\omega)=E_B^{dc}(1+\omega^2\tau_c^2)^{1/2} \tag{1}$$

has been used to predict the frequency dependence of laser-induced breakdown in the region of departure from the dc limit. In Fig. 1 the solid segment and its dotted extension have the form of Eq. (1). The aforementioned increase in the NaF threshold at 6943 Å indicates that $h\tau_c^{-1}\simeq\hbar\omega_{ruby}$ (1.79 eV) in NaF, and roughly indicates the $h\tau_c^{-1}$ position on the $\hbar\omega$ axis of Fig. 1. The dashed curve outlines the frequency dependence of the Keldysh tunneling mechanism.[20] As the photon energy becomes sizable compared to the material band gap, this tunneling mechanism is described as multiphoton ionization. At some point in this transition the multiphoton ionization probability becomes large enough to effectively assist the breakdown process, still classifiable mainly as avalanche ionization. Several papers[21-23] recently have considered aspects of this combination process. One immediate consequence of the multiphoton ionization assistance is the ready supply of initial electrons with which the breakdown process may proceed. For sufficiently lower frequencies, the productions of such electrons is a subtle matter. As the photon energy exceeds $\frac{1}{3}\mathcal{E}_G$, we expect the threshold to reverse its trend as the arrow indicates in Fig. 1. As the photon energy is increased beyond $\frac{1}{2}\mathcal{E}_G$, copious two-photon absorption (this process will henceforth be abbreviated as 2PA) will occur. At such frequencies, breakdown experiments utilizing an external focusing lens will be complicated considerably by 2PA energy depletion and distortion of the laser pulse in the medium before the lens focal region.

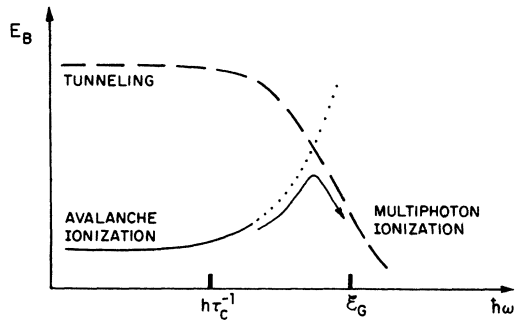

FIG. 1. Schematic frequency dependence of the two intrinsic physical processes involved in laser-induced breakdown: avalanche ionization and multiphoton absorption ionization. ($\mathcal{E}_G$ denotes the optical band gap of the material and $h\tau_c^{-1}$ the energy associated with the electron collision time τ_c.) The solid curve is the region of investigation prior to this study. The present work investigates the region located by the arrow.

One should note the manner in which the two curves in Fig. 1 will shift horizontally as the material parameters $\mathcal{E}_G$ and $h\tau_c^{-1}$ are changed and $\hbar\omega$ is held fixed. Because $h\tau_c^{-1}$ is likely to be less sensitive to $\mathcal{E}_G$ than is the threshold for strong multiphoton absorption, the most demonstrative effect on Fig. 1 from changing to a material with larger $\mathcal{E}_G$ would be the shift of the dashed curve to the right and creation of a larger hump in the composite threshold trajectory. Therefore a comparison of breakdown thresholds at two different laser frequencies, both in the region of the transitional hump, for a series of materials and band gap, would provide a test of the surmised behavior which is illustrated in Fig. 1. From our picture, one would expect from such a comparison to see a systematic increase in $E_B(\omega_2)/E_B(\omega_1)$, where $\omega_2>\omega_1$, as a function of material band gap. We will present data later in this paper which depict just such a systematic increase.

A recent review of dielectric breakdown induced by laser pulses is found in Ref. 19. Recent theoretical papers which will serve as well to introduce the reader to segments of the literature are found in Ref. 24 by Holway and Fradin and Ref. 25 by Sparks and Duthler. Numerous papers concerning all aspects of laser-induced dielectric breakdown appear in National Bureau of Standards Special Publications.[26] The 1973 edition of O'Dwyer's book[27] may be consulted for information on dc, as well as high-frequency, breakdown phenomena.

Section II outlines the theory necessary for the evaluation of our experiments. Section III relates the experiment and results of the 5321-Å study.

The 3547-Å experiment and results are described in Sec. IV. Comparison of our experimental results with theories on multiphoton contributions to breakdown[4,21] are given in Sec. V, and a summation is found in Sec. VI.

II. THEORY

The objective of our experiment is to obtain the high electric fields requisite for breakdown, while at the same time minimizing the input pulse power and thus the effects of self-focusing. This we do by tightly focusing the laser pulses into the sample with short focal length lenses. In the absence of any self-focusing, we know that a diffraction-limited light pulse with a Gaussian spatial intensity distribution of radius ρ [$I(r) = I_0 \exp - (r/\rho)^2$], focused by a lens of focal length f, will produce an intensity distribution in the focal plane of

$$I_f(r) = (P/A)e^{-(r/w)^2} . \tag{2}$$

Here P is the pulse peak power, defined as

$$P = 2\pi \int_0^\infty dr\, rI(r) , \tag{3}$$

where $A = \pi w^2$, and $w = \lambda f/2\pi\rho$ if λ is the light wavelength in air. In addition, we know that if the power P in the light pulse exceeds some fraction of the critical power value known as P_1,[28] defined as

$$P_1 = c\lambda^2/32\pi^2 n_2 \tag{4}$$

for a Gaussian pulse, the above focusing behavior is modified by self-focusing. The material parameter which determines P_1 is n_2, the nonlinear refractive index. If E is the rms field amplitude and n is the total refractive index, n_2 is defined via $n = n_0 + n_2E^2 + \cdots$. The equations above may be altered to account for self-focusing with the help of the analytical "aberrationless" or "constant shape" (CS) approximate theory[28-30] if P is "less than" P_1. In that case, Eq. (2) becomes

$$I_f(r) = (P/A)(1 - P/P_1)^{-1} e^{-(r/w)^2} . \tag{5}$$

Depending on whether P_1 is known for a given material of interest, Eq. (5) may be used in two different ways for breakdown threshold measurements.

If n_2 and thus P_1 are not known, then Eq. (5) may be used to measure both the breakdown threshold electric field E_B and P_1, simultaneously, as was done by others[31-33] and by ourselves in earlier 1.064-μm studies.[1,2] In that situation, lenses of different focal area A_i are used to produce breakdown at the focal point, each lens requiring a different input power P_i. One may then plot the various reciprocal input powers P_i^{-1} versus the respective focal areas A_i^{-1}. As long as all P_i are much "less than" P_1 (an unknown), the points will define a straight line, as indicated by Eq. (5). Figure 2 indicates these features schematically. There the slope of the solid line is $I_f(0)^{-1}$ (and equals the reciprocal breakdown intensity at threshold) and E_B is obtained using the relation $E_B = [I_f(0)/n_0\epsilon_0 c]^{1/2}$, where n_0 is the linear refractive index, ϵ_0 is the free-space permittivity, and c is the vacuum speed of light. The intercept of the line with the P^{-1} axis yields P_1^{-1}. If, however, n_2 is known, then the threshold power measurement from only one lens suffices to determine E_B from Eq. (5). It should be stated that the slope-intercept, controlled breakdown method discussed here and previously is an intrinsically less accurate way to measure n_2 than some other available schemes.[34-39] It is, nevertheless, in the face of unknown n_2 values, the only known way to obtain bulk breakdown threshold measurements in the picosecond pulse regime which are corrected for self-focusing.

Aside from the paucity of accurate available n_2 values, another situation exists which thwarts the extension of picosecond breakdown measurements to shorter optical (uv) frequencies. All the above discussion was based on input pulse powers P being "less than" P_1, the critical power for the onset of self-focusing by paraxial rays in an unfocused geometry. The problem lies in our inability to ascribe more precision to the phrase "less than" in the previous sentence. It is not

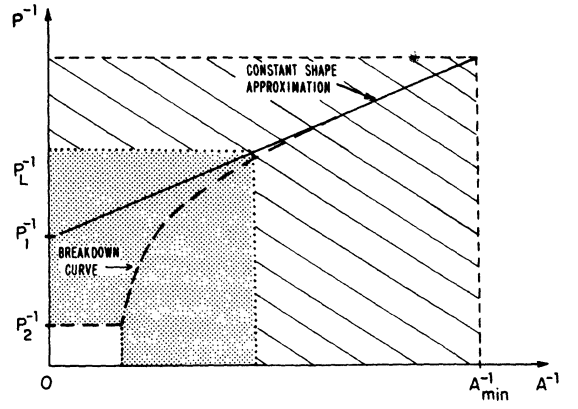

FIG. 2. Illustrations of the slope-intercept breakdown construction, as given by Eqs. (5) and (6), wherein one plots for a given lens the reciprocal pulse input power (P^{-1}) versus reciprocal focal area (A^{-1}). The dashed curve is defined by the breakdown and self-focusing properties of the material, and the solid line is from the constant shape approximation. P_1 and P_2 are the "paraxial" and the "catastrophic" critical powers, respectively. See Sec. II for a discussion of the two curves. A_{min} is the minimum focal area obtainable with a given wavelength.

known quantitatively how, in the focused geometry (where an external lens focuses the light pulse into the material sample), the constant shape approximation breaks down as P approaches and, moreover, exceeds P_1. Figure 2 illustrates our present understanding of this behavior. The cross-hatched area is the region of validity of the CS approximation. The dashed curve is the locus of (A^{-1}, P^{-1}) points defined by the breakdown threshold of a particular material. The straight line, which is asymptotic to the dashed curve in the low-power limit, is defined by Eq. (5) and is the construction used in our previous papers[1,2] to measure P_1. The dotted area in the figure is the region within which the self-focusing behavior has departed from the CS description. The exact functional form of this departure, and thus of the dashed breakdown curve in the dotted region, is not known. Therefore, the exact limiting power level (indicated by P_L^{-1} in Fig. 2), beyond which one should not apply the constant-shape approximation to deduce breakdown thresholds, is not known. It is indicated by careful numerical calculation[28] that the power in a Gaussian pulse must exceed P_1 by a factor of 3.7 before a catastrophic self-focus (a singularity in axial intensity) will occur, in either externally focused or unfocused geometry. This intensity singularity manifests itself by breakdown and other processes, and represents the horizontal segment of the breakdown curve in Fig. 2. This multiple of P_1 leading to the singularity is denoted in the literature by P_2. For pulse powers very near to but less than P_2, the maximum axial intensity may be expressed then by Eq. (5) with P_1 replaced by P_2.[28] And in fact, the maximum axial intensity reached at any input power level might be expressed by the relation

$$I_{\max} = (P/A)[1 - P/\phi(P)P_1]^{-1}. \quad (6)$$

Here $\phi(P)$ is presently unknown and must be the result of numerical calculation, but will behave monotonically between the following limits:

$$\phi(P) \to 1 \quad \text{for } P \ll P_1,$$

$$\phi(P) \to 3.7 \quad \text{as } P \to P_2.$$

Data published by Marburger[28] indicates that efforts may be made to compute the function $\phi(P)$. Such new results, in a form applicable to any focusing geometry, would be of great use for experiments of many types, especially with higher laser frequencies considering the restricting λ^2 dependence of P_1. Knowledge of $\phi(P)$ would, for example, remove our present dependence on the CS approximation and allow more than four times more power to be used to produce calculable intensities for breakdown studies such as this one. In that case the segment of the breakdown curve within the dotted area and down to the P_2^{-1} level would be usable. Similar applications could be made to studies of absolute coefficients for uv two-photon absorption in solids and liquids, etc. The data presented in this paper will be tabulated so that the breakdown threshold values may be recalculated by the reader in the future, should data on the $\phi(P)$ function appear.

III. BREAKDOWN STUDY AT 5321 Å

A. Experiment

1. Apparatus

The experimental arrangement is shown in Fig. 3 and is in large part the same as used in Refs. 1–3. The YAlG:Nd laser oscillator is mode-locked by saturable absorber (Kodak 9860). It produces a train of TEM_∞ transverse mode, 1.064-μm pulses of 30-psec average duration. One of these pulses is selected for use by a KH_2PO_4 Pockels cell which is driven by a laser-triggered spark gap. The selected pulse is then monitored for proper switch-out behavior on a Tektronix 519 oscilloscope (CRO 1). Photodiodes P2 and P3 measure the energy content in two samples from the main pulse, one at 1.064 μm and the other converted to 5321 Å by a KH_2PO_4 crystal. From these two signals we obtain the temporal duration of each individual picosecond laser pulse.[40] With

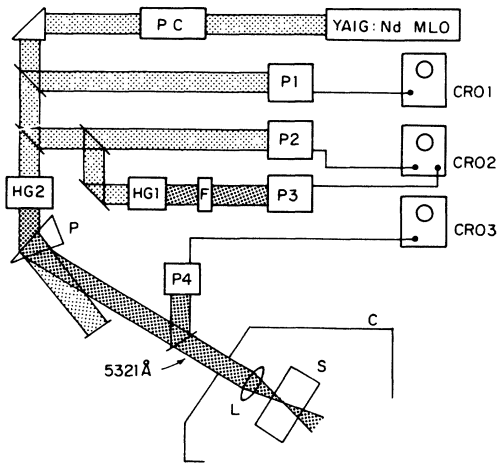

FIG. 3. Schematic diagram of the experimental apparatus. Notation: MLO, mode-locked YAlG:Nd laser oscillator; PC, Pockels cell single pulse selector; P1–P4, photodiode detectors; CRO1, Tektronix 519 oscilloscope; CRO 2-3, Tektronix 555 oscilloscopes; HG1, KH_2PO_4 5321-Å generation cell; HG2, CsH_2AsO_4 temperature-tuned 5321-Å generation cell; F, green-pass filter; P, dispersing prism; C, curtain; L, lens; S, material sample.

this temporal characterization, the main part of the infrared pulse is converted to a 5321-Å pulse by harmonic generation cell (HG2) containing a cesium dihydrogen arsenate crystal. The crystal is maintained in an oven at the proper temperature for noncritical or 90° phase matching. Two characteristics of the green pulse, crucial for this experiment, accrue from 90° phase matching.[41] First, no spatial distortion of the green pulse occurs by "walk-off," as occurs with angle-tuned phase matching (see Sec. IV). The 5321-Å pulse is cylindrically symmetric, without spatial noise, and Gaussian in shape. Figure 4 is a tracing of an oscillogram from a Reticon linear photodiode array (Reticon Corp., Sunnyvale, Calif.) of a typical green pulse profile. The waveform was smoothed by no more than the width of the tracing pen. Such a distortion-free profile is required for accurate calculation of the electric field distribution of a laser pulse in the focal region of a lens. Second, this harmonic generator produces, for an unlimited length of time, green pulses with the same spatial profile. Such reproducible behavior, over a period of several hours and from day to day, is difficult, if not impossible, to obtain from angle phase-matched crystals. A serious attempt was made by us,[42] prior to the present experiment, to accurately measure breakdown thresholds with 5321-Å pulses generated in an angle-tuned KH_2PO_4 crystal. The effort was not satisfactory for the reasons outlined above. The same set of difficulties interfered with our efforts to study breakdown at the third-harmonic frequency of the YAlG:Nd laser, as related in Sec. IV.

The 5321-Å pulse is separated from the infrared pulse by a prism, oriented to maintain the circular cross section of the green pulse. Photodiode P4 monitors the absolute energy content of the green pulse just before the focusing lens L. Photodiode P4 was calibrated with two Eppley Laboratory (Newport, R. I.) thermopiles, themselves calibrated against National Bureau of Standards sources. By using the energy content signal from P4 and the individual pulse duration which we derive from P2 and P3 signals, we obtain the peak power in each individual pulse. The measured full angle of divergence of the harmonic pulses is less than 0.9 mrad. By measuring the cross-sectional area of the pulses at the lens position with the linear photodiode array, and using the design parameters of the lens, we may calculate the area in the focal plane of the lens.[1] The measurements which we report here were made with a 1.0-in. focal length corrected lens, with a calculated focal area (defined as πw^2, where w is the e^{-1} radius of intensity) of 14.8 μm^2. This figure includes contributions from spherical aberration of the lens and the planar sample surface,[1] both of which amounted to a calculated correction to the area of less than 2%. This calculated focal area was checked experimentally by a scanning aperture technique.[1] To within the limiting accuracy of the technique, ±20%, the experimental and calculated areas agreed.

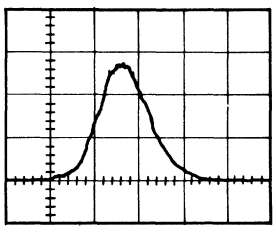

FIG. 4. Oscillogram tracing of the spatial intensity profile of the 5321-Å pulses produced by the CsH_2AsO_4 crystal. The oscillogram was recorded with a commercial linear array of 256 photodiodes with 0.05-mm resolution.

We have employed an average full width at half intensity duration of 21 psec for our 5321-Å pulses. This duration is shorter than the 30-psec parent pulse duration by $1/\sqrt{2}$, as given by the theory for the ideal frequency doubling of Gaussian pulses in the low conversion efficiency regime. Final individual pulse durations were calculated using this average duration value, the τA technique,[40] and a computer program to account for the temporal stretching of the pulse due to saturation of the conversion efficiency. This last correction is discussed in Sec. III B1.

2. Procedure

The procedure for each measurement began with the alignment of a sample (dimensions typically $6 \times 20 \times 30$ mm^3) in the x-y translating holder so that the pulse propagation direction was normal to the sample face. Then the lens itself was aligned with a reproducible procedure, discussed previously,[1] which was made easier by the visibility of the light in the present experiment. The typical location of the focal point was 2 mm inside the sample front surface. Next the sample was checked for unacceptable surface polishing roughness, a check which was not possible with invisible 1.064-μm light. Shots were fired through the sample, below the breakdown threshold, and the transmitted light was observed on a card. If the transmitted light pattern showed a contribution due to diffraction from polishing scratches, the sample was either repolished until no surface scratch diffraction was observed, or the sample was deleted from the experiment if sufficient smoothness was unobtainable. The polishing was performed by an experienced technician using synthetic lap material and alumina abrasive particles down to 0.05 μm diameter. Several mate-

rials were unfortunately eliminated due to this problem—the relatively soft, small-band-gap materials including NaBr, KBr, and KI. It now appears that such surface distortion may have been the cause of the heretofore unexplained rise in the breakdown thresholds, relative to NaCl, of KBr, KI at[1] 1.06 μm and[11] 6943 Å over their values at dc and 10.6 μm. The absence of this problem in another study[10] at 1.06 μm is not understood. At 10.6 μm,[9] however, such submicron roughness would have almost no distorting effect.

After a proper sample and the lens were aligned, a series of 50–100 shots were fired into sites with recorded location in the sample, *one shot per site*, as was the procedure in our 1.064-μm studies.[1-3] The pulse power was increased throughout the series, by altering the Pockels cell voltage which changes the position of switch-out from the oscillator train. In contrast to Nd:glass mode-locked lasers, YAlG:Nd laser pulses do not vary in duration as a function of pulse position in the train. For each shot, signals from detectors P2, P3, and P4 were recorded and visual observation of microspark formation was used to indicate whether breakdown occurred on each shot. Such visual sightings were not used to determine the breakdown threshold, however. If one wishes to meaningfully compare thresholds measured at different light wavelengths, then the threshold observation mechanism cannot itself be wavelength dependent. The ocular observation of spark production (with its attendant scattering of subsequently arriving laser light) would be particularly subjective and wavelength dependent between 1.064 μm and 5321 Å. So the threshold here was defined by the same criterion as used in our previous 1.064-μm study, namely as the minimum electric field value, reached at the focal point and at the peak of the pulse, which produced microscopically observable, permanent damage in the material. The microscopic observation of the matrix of sites was performed after completion of the laser irradiation.

Although the visual sightings of spark formation were not appropriate for identification of breakdown thresholds, the visual thresholds obtained with the 1.0-in. focal length lens, and also with 1.5- and 3.0-in. focal length lenses, were recorded for each material. The calculated focal areas of the two latter lenses were 32.9 and 131.1 μm^2, respectively. These visual thresholds were used to investigate self-focusing behavior for pulses having powers between P_1 and P_2. Discussion of that behavior is found later in Sec. III B 2.

At least three different experimental runs were made on each tested material with each lens to ascertain the threshold reproducibility.

B. Results of the 5321-Å study

1. Dielectric-breakdown threshold data

In this section we will present and discuss new results for dielectric breakdown thresholds at 5321 Å, induced by our nominally 21-psec pulses.

Several general characteristics of this damage study were observed to be the same as those encountered in Refs. 1–3. The thresholds were again noted to be *sharply* defined.[23] That is, our resolution of the thresholds was limited by our experimental uncertainty and reproducibility, which was observed to be ±15%. Again, only rare evidence of the presence or influence of inclusions was observed in the experiment or under the microscope ($\lesssim$1% of the sites). Again, the results did not vary from site to site within a sample, or among different samples of the same material, by amounts larger than our experimental uncertainty. Figure 5 exhibits the morphology in two of the sample materials, KH_2PO_4 and LiF. These breakdown sites were photographed with blue light on a Leitz microscope at 250-power magnification and ~0.8-μm resolution. The focal spot radius to the $1/e$ point of the electric field ($\sqrt{2}w$) is 3.1 μm, and the Rayleigh distance for the electric field (given by $\pi n_0 w^2/\lambda$) is approximately 85 μm. The scale markers in the figure represent a 10 μm distance. The laser pulses which caused the damage of Figs. 5(a) and 5(b) had maximum focal point electric fields of approximately 14 and 40% above the respective thresholds for the two materials. The typical microscopically observed damage morphology of Fig. 5 is similar to that reported earlier[3] at 1.064 μm. Except for rare impurity sightings, damage always occurred within a needle shaped volume along the propagation axis at the focal point, the dimensions of which were only ~1 by ~10 μm at threshold. The perimeter of this damage was nonlinearly correlated with the inci-

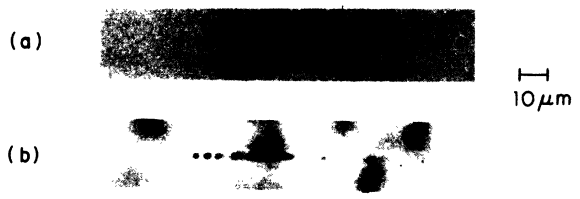

FIG. 5. Breakdown morphology in (a) KH_2PO_4 and (b) LiF, induced by 5321-Å picosecond laser pulses focused to an e^{-1} rms electric field focal radius of 3.1 μm. The scale markers denote a distance of 10 μm, and the pulses were incident from the left-hand side. The maximum rms electric field reached at the focal point for photographs (a) and (b) were 14 and 40% above the respective thresholds for the two materials. The mottled background appearance in (b) is immaterial.

TABLE I. 5321-Å test material parameters.

Material	$\mathcal{E}_G$ (eV)	n_0	n_2 (10^{-13} esu)	P_1 (kW)	P_2 (kW)
KH_2PO_4	6.92	1.5126	1.00 ± 0.30 [a]	267	988
SiO_2	7.8	1.4608	1.00 ± 0.08 [b]	281	1040
NaCl	8.7	1.5491	4.20 ± 0.84 [c]	64	238
CaF_2	10.0	1.4354	1.13 ± 0.34 [d]	237	877
NaF	11.0	1.3269	0.94 ± 0.47 [e]	283	1047
LiF	12.0	1.3937	0.92 ± 0.16 [d]	290	1073

[a] Reference 39.
[b] Reference 35.
[c] Reference 34.
[d] Reference 36.
[e] Reference 1.

dent electric field strength, again as encountered at 1.064 μm. Within the damage perimeter occurred nucleation sites of $\lesssim 1$ μm diameter at a density of $\sim 10^{10}$ cm^{-3} at threshold. No major differences were observed, between 1.064- and 0.532-μm morphology, which indicates that the final stages of the damage process are still due to avalanche ionization. A major difference in morphology would indicate massive or dominant influence from multiphoton ionization processes.

Table I lists several material parameters for the six tested dielectrics: KH_2PO_4, SiO_2 (fused), NaCl, CaF_2, NaF, and LiF. All the crystalline (monocrystalline) samples were cut so that the laser pulses propagated along the [001] axis, with the electric vector along the [100] axis. The KH_2PO_4 samples were purchased from Cleveland Crystal Co. (Cleveland, Ohio), while the other crystalline materials were purchased from Harshaw Chemical Co. (Solon, Ohio). The fused SiO_2 samples are Suprasil I, purchased from Amersil, Inc. (Hillside, N. J.). Column 2 of Table I lists band gap ($\mathcal{E}_G$) values, all of which (except that for KH_2PO_4) were obtained from standard reference books or manufacturer's data. For KH_2PO_4, we were unable to find either $\mathcal{E}_G$ or optical absorption data in the ultraviolet beyond 2100 Å,[43] which indicates a disturbing lack of knowledge of impurity absorption behavior of this important material in the uv. An ultraviolet spectrogram of our own samples indicates[44] strong absorption beginning at about 1800 Å, or 6.92 eV. For convenience, column 3 lists linear refractive index data, which is needed to convert nonlinear refractive index data (column 4) to third-order nonlinear optical susceptibility ($\chi^{(3)}$) data, for comparison with data published elsewhere [$n_2 = 12\pi n_0^{-1}\chi^{(3)}_{xxxx}(-\omega, \omega, \omega, -\omega)$]. For KH_2PO_4 and CaF_2, ordinary ray n_0 values are appropriate. In column 4, we list the most accurate n_2 values available from the literature for our materials, according to their quoted uncertainties which range between ±8 and ±50%. The last two columns tabulate the critical powers P_1 and P_2, which differ by a factor of 3.7 as discussed earlier.

In Table II we present the new breakdown threshold results at 5321 Å along with comparison data at 1.064 μm. The second column lists values of input power P at breakdown threshold. The ratio of these power thresholds to the respective P_1 critical power values from Table I are listed in the third column. The aforementioned focal area of 14.8 μm^2 was corrected slightly ($\lesssim 9\%$) for each material to account for saturation[45] of the conversion efficiency of 1.064-μm light to the second harmonic. These power dependent correction factors were computed by numerical solution of the harmonic generation equations including pump beam depletion. The actual focal area values used are listed in column 4 of Table II. This spatial broadening (the profile remains Gaussian to a good approximation) due to conversion saturation also lengthens the pulse temporally. All power values in this paper have been corrected by the appropriate small factors ($\lesssim 5\%$), obtained from the same numerical computation.

The values of P, P_1, A, and n_0 from the tables suffice to determine E_B using Eq. (5). The new values so obtained from our studies for the breakdown rms electric field strength, at 5321 Å with nominally 21-psec pulses, are denoted $E_B^{\mathcal{E}}$ (21

TABLE II. 5321-Å dielectric-breakdown threshold results.

Material	P (kW)	P/P_1	A (μm^2)	$E_B^{\mathcal{E}}$ (21 psec) (MV/cm)	E_B^{ir} (30 psec) [a] (MV/cm)	E_B^{ir} (21 psec) (MV/cm)	Δ_1 [b]
KH_2PO_4	151.2	0.57	16.0	23.4	22.3	33.6	0.70
SiO_2	129.0	0.46	15.9	19.0	11.7	17.6	1.08
NaCl	38.4	0.60	15.1	12.4	7.3	11.0	1.13
CaF_2	146.0	0.62	15.9	25.2	14.4	21.7	1.16
NaF	126.4	0.45	15.8	19.4	10.8	16.3	1.19
LiF	171.3	0.59	16.1	26.5	12.2	18.4	1.44

[a] Reference 1.
[b] The quantity Δ_1 is defined as $E_B^{\mathcal{E}}$ (21 psec)/E_B^{ir} (21 psec).

psec) and listed in column 5 of Table II. The superscript g denotes the green wavelength. The thresholds range from a low of 12.4 MV/cm for NaCl to a high of 26.5 MV/cm for LiF.

The discussion of the uncertainty in the E_B^g (21 psec) values of Table II is complicated by the unavailability of $\phi(P)$ data. Our experimental conditions allow us to know the $(P/A)^{1/2}$ factor in the expression for E_B [Eq. (6)] to an estimated ±15%. The absence of $\phi(P)$ data has no effect on the reproducibility of our thresholds, of course, and our experimentally observed reproducibility limit of ~±15% at 5321 Å reflects that fact. The absence of $\phi(P)$ data does, however, compound the uncertainty in the absolute numbers which are listed in Table II for E_B^g (21 psec). In column three of Table II, the P/P_1 values range from 0.45 to 0.62, and it is plausible that they are too large to permit the CS approximation to yield high accuracy for the breakdown threshold electric fields from Eq. (5). For that reason we will later consider the full range of possible modification of our results, which in the worst case would be obtained by using P_2 in the denominator of Eq. (5) in place of P_1. For the present, however, we will continue to discuss E_B values obtained with P_1 in Eq. (5) [$\phi(P)=1$] in the CS approximation.

Our greatest interest lies in determining what effect the doubling of the light frequency has had on these thresholds, by comparing them with the results of our previous study at 1.064 μm.[1] Column 6 of Table II lists the thresholds from that infrared study [denoted E_B^{ir} (30 psec)]. As indicated by the notation, the ir data was taken with nominally 30-psec duration pulses, and it is desirable to separate out the pulse-duration-dependent changes in these two sets of data so that we may observe changes due to light frequency, or photon energy, only. In order to convert the E_B^{ir} (30 psec) data to E_B^{ir} (21 psec) data, we require the pulse-duration dependence in the picosecond range of the breakdown threshold for the six materials tested. Unfortunately such data is known[1] only for NaCl and, to a lesser degree, for five other alkali halides. We are restricted, therefore, to an approximate treatment for removal of the pulse-duration dependence, based on NaCl data only. From Fig. 6 of Ref. 1, one obtains that the ratio of E_B^{ir} (21 psec) to E_B^{ir} (30 psec) for NaCl is about 11/7.3 = 1.51. We have used this number to convert the entries of column 6, Table II, to those of column 7. It is, of course, unlikely that the threshold dependence on pulse duration would be exactly the same for the dissimilar collection of tested materials. However, over such a small range of pulse duration (30–21 psec), the use of a sirgle renormalization factor is reasonable. In that case, the change in breakdown thresholds due to frequency alone, denoted Δ_1, is the ratio E_B^g (21 psec)/E_B^{ir} (21 psec), and is listed in the final column of Table II. As discussed in Sec. I, the systematic variation of Δ_1 with optical band gap should indicate the presence, if any, of frequency-dependent or quantum effects. Such systematic variation has never before been seen in experiments on bulk laser-induced breakdown. Figure 6 illustrates this point. In that illustration we have ordered the alkali halides according to band gap. Plotted along the vertical axis is the ratio of breakdown thresholds from two previous experiments, one at 1.06 μm,[10] with ~5.0-nsec laser pulses [E_B^{ir} (5 nsec)], and the other at[6] dc (E_B^{dc}). No systematic behavior of this ratio is observed, and the same is true for any other pair of laser-induced breakdown experiments reported thus far. The basis for this frequency-independent behavior up to 1.064 μm has been discussed previously[19] and is due largely to the two conditions mentioned in Sec. I concerning the brevity of the hot-electron collision time and the size of the band gap in these solids. Even the smallest band gap of 6.2 eV for the tested alkali halides in the previous 1.064-μm experiments would require at least six photons for the occurrence of direct multiphoton transitions, and such transitions are vanishingly small even at breakdown intensity levels. At the ruby laser frequency (1.79-eV photon energy), four photons are needed to directly cross a 6.2-eV band gap and the probability is still small. At a 1.79- or 1.17-eV photon energy, it is probable that the only important role in the breakdown process in these insulators played by multiphoton transitions is the supply of avalanche initiating electrons by the two-photon ionization of defect centers.[21] As mentioned earlier, from our own

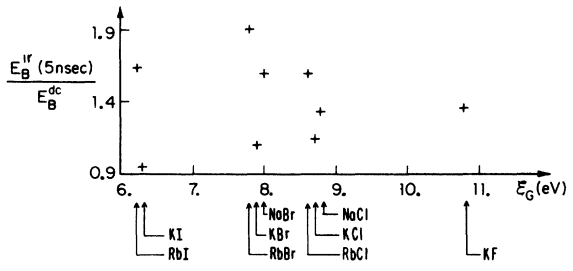

FIG. 6. Illustration of the absence of multiphoton effects in insulator breakdown threshold data for wavelengths down to 1.064 μm. The ratio of thresholds at the Nd frequency (Ref. 10) to that at zero frequency (Ref. 6) is plotted versus alkali halide band gap. No systematic pattern is evident, in contrast with the higher frequency data of Fig. 7.

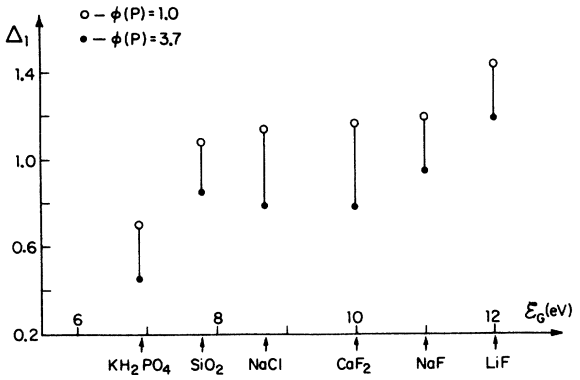

FIG. 7. Illustration of the band-gap-dependent behavior of the threshold change Δ_1 observed in the 5321-Å experiment. Here Δ_1 is the ratio E_B^{ξ} (21 psec)/E_B^{1r} (21 psec) from Table II, plotted versus band gap ($\mathcal{E}_G$) for the six test materials. For each material, the open circle point and the dotted point result from the use of $\phi(P)=1$ and $\phi(P)=3.7$ in Eq. (6), respectively, to determine E_B^{ξ} (21 psec). The discussion of the trend of this data is found in Sec. IIB1.

work in the present and previous[1] studies, it appears now that the unexplained increases in the thresholds (relative to that of NaCl) encountered by Fradin and Bass[11] at 6943 Å and by us[1] at 1.064 μm in soft, low-band-gap ($\lesssim$8 eV) alkali halides may have been an artifact due to the undetected sample surface roughness mentioned earlier. They[11] also reported a large increase in the breakdown threshold of NaF over that of NaCl at 6943 Å, and it is likely that most of that increase is a true observation, indicating the condition $\omega\tau_c \gtrsim 1$ as discussed in Sec. I. This observation indeed indicated the departure of the breakdown process from the dc limit at 6943 Å. Up to the present 5321-Å experiment, the NaF observation of Fradin and Bass was the only experimental datum point available for checking the predictions of frequency dependence summarized in Fig. 1.

Now let us discuss the frequency-dependent threshold changes encountered in this study at 5321 Å (2.33 eV). We plot in Fig. 7 the values of Δ_1 listed in Table II versus material band gap $\mathcal{E}_G$. Because of the specific uncertainty introduced by the lack of $\phi(P)$ data, we have plotted in addition the Δ_1 values obtained by using in each case P_2 in Eq. (5), rather than P_1. Due to the closeness of the P/P_1 values for the six materials (see Table II), it is probable that the true data points, were $\phi(P)$ known, would lie almost the same relative distance between the circle points and the solid points. That is, the adjustment of the circle points to their true location in Fig. 7 due to full knowledge of $\phi(P)$ would probably result in only a small, nearly constant lowering of the circle points. (Nevertheless, all information necessary to make such an adjustment in the future is given in this paper.)

The variation of Δ_1, the frequency-dependent change in the 5321-Å and 1.064-μm breakdown thresholds, with material band gap in Fig. 7 is unmistakable. A Δ_1 ordinate of 1.0 indicates no change in threshold on doubling the light frequency. The exact position of 1.0 on the vertical axis is not known due to the uncertainty introduced by the E_B^{1r} (21 psec) renormalization. Nevertheless, the data of Fig. 7 indicate that the band gap value for a Δ_1 of unity is approximately 7.5 eV. The energy of 3 photons of 5321-Å light is 7.0 eV. Thus, for materials with $\mathcal{E}_G < 7$ eV, the influence of multiphoton transitions dominates over the competing effect of the light frequency exceeding the avalanche collision time of hot electrons: the result is $\Delta_1 < 1$. For KH_2PO_4, we obtain a Δ_1 of 0.70 which is a frequency-dependent decrease of 30%. For materials with $\mathcal{E}_G > 7$ eV, 4 or higher-order multiphoton transitions (neglecting defect populations) are less effective against the $\omega\tau_c$ increase at 5321 Å, and Δ_1 values exceeding unity are the result. A maximum Δ_1 value of 1.44 is registered for LiF, a material ($\mathcal{E}_G \simeq 12.0$ eV) unaffected by interband multiphoton transitions at 5321 Å.

It is perhaps instructive to consider the Keldysh model[20] for an indication of the relative strengths of multiphoton transition effects in our materials. The Keldysh model allows one to estimate for a particular field strength, the transition rate per unit of volume and time for the promotion of electrons from the valence band directly to the conduction band via the lowest-order, energetically sufficient, multiphoton transition process. We have used the free-electron mass, in place of the unknown effective mass, the band-gap values listed in Table I, and the breakdown threshold field strengths from Table II [E_B^{ξ} (21 psec)] to calculate the Keldysh rates. Here, because we wish only to consider the rough variation of this rate for our six materials, such a single field strength estimation will suffice in lieu of a detailed computation. The Keldysh rate for KH_2PO_4, at 23.4 MV/cm, with $\hbar\omega = 2.33$ eV, is large ($\sim 7\times 10^{28}$/cm^3 sec) due to the fact that $3\hbar\omega$ slightly exceeds the band gap. As we go to SiO_2 at a field strength of 19.0 MV/cm the rate drops by a factor of over 660 as the lowest-order transition then requires four photons. The further successive decreases in the rate as one proceeds through NaCl, CaF_2, NaF, and LiF are less pronounced: 46, 2, 21, 20, respectively. The trend of these numbers is reflected in the Δ_1 data of Fig. 7. The much greater strength of the three-photon transition for KH_2PO_4,

compared to the higher-order transition for the other materials, is consistent with the significantly lower Δ_1 value for that material from our experiment. The gradual increase in the Δ_1 value for $\mathcal{E}_G > 7$ eV is consistent not only with the gradual weakening of the higher-order transition probabilities, but also with the "low"-frequency avalanche ionization, Joule heating model embodied in Eq. (1). Thus one sees that the data of Fig. 7 illustrates the continuous evolution of the character of the breakdown process as a function of material band gap from the "pure" avalanche ionization, Joule heating region of large $\mathcal{E}_G$ into the regime where the influence of multiphoton transitions is observable.

2. *Self-focusing behavior*

The 5321-Å experiments reported here provide qualitative verification of two aspects of self-focusing behavior in the tightly focused geometry, which to our knowledge were not investigated before. For the self-focusing experiments, we used the same experimental arrangement as in Fig. 3. However, three different lenses (focal lengths 1.0, 1.5, 3.0 in.) were used rather than one as in the previous Sec. III B1. Pulses of increasing power were passed with each lens into the sample materials, one shot per site, and the threshold power for the production of a visible, light-scattering plasma at the focal point was recorded. Note that this criterion for plasma scattering (PS) is not identical to the criterion for threshold breakdown as discussed in Sec. III A2. Great care was necessary to remove extraneous scattered light so that only the focal volume was observed. Considering the sensitivity of the eye at 5321 Å to scattered photons, one would not be surprised that the PS criterion required less power to achieve than the breakdown criterion of permanent microscopic damage. For the 1.0-in. focal length lens which was used for both experiments, the ratio of the PS threshold power to the breakdown threshold power varied with material between about 1.0 and 0.5. Nevertheless, the experiments showed that the PS criterion was sufficient to indicate reproducibly the attainment of a well-defined electric field in the sample. Because it is less time consuming to implement, the PS criterion enabled several materials to be examined.

TABLE III. Self-focusing data for SiO_2 (5321-Å study).

f (in.)	A (μm^2)	P (kW)	P/P_1	P/P_2
1.0	15.9	138.9	0.49	0.13
1.5	36.6	260.2	0.93	0.25
3.0	155.7	709.1	2.52	0.68

$P_{int} = 1138$ kW

$P_{int}/P_2 = 1.09$

By plotting the PS power thresholds versus focal area for the three lenses, as discussed earlier and illustrated in Fig. 2, we investigated the trajectory of the breakdown curve in the dotted region of that figure. Referring to Fig. 2, consider the analysis of a data set with points lying both above and in the power range P_1^{-1} to P_2^{-1}. A straight line fit to those points will yield a vertical axis intercept below P_1^{-1} and, perhaps, even below P_2^{-1}, if the construction in the dotted region of Fig. 2 is correct. Our data for a typical material, SiO_2, are shown in Table III. The calculated focal areas, corrected for saturation as mentioned earlier, are listed in column 2, and PS power thresholds are listed in column 3. Columns 4 and 5 indicate that the power values almost span the P_1 to P_2 region. If one plots these data as in Fig. 2, and fits a straight line to the three points, the intercept of the line with the P^{-1} axis yields a value P_{int} of 1138 kW. As stated in Table III, this quantity indeed exceeds P_2, verifying qualitatively the construction of the dashed breakdown curve as drawn in Fig. 2. A great need exists for accurate numerical computational results of $\phi(P)$ with which the data of Table III could be further tested.

The second aspect of self-focusing behavior which has been qualitatively verified in our experiments concerns the exact input power value, in the tightly focused geometry, which will result in a singularity in axial intensity. In numerical computations, such a singularity is recognized as a rapid increase in intensity of orders of magnitude with only a small incremental increase in input power.[28] In the experimental situation, the singularity is restricted to the breakdown intensity. As listed in Table III, in SiO_2 we were able to focus up to 0.68 of P_2 before initiating a sizable plasma density. Of the six materials we tested, P/P_2 for the 3-in. lens was highest for SiO_2. The other materials registered P/P_2 between 0.32 and 0.57 for the 3-in. lens. All these P/P_2 values correspond to P/P_1 values exceeding unity. Therefore, we have verified that in the tight externally focused geometry, as discussed by Marburger,[28] power of P_1 is insufficient to produce a self-focus singularity. We were not able with our lenses to verify that the full P_2 is so required, but we did determine that at least ~0.7 of P_2 is required. This data could be extended further, of course, with longer focal length precision lenses.

IV. BREAKDOWN STUDY AT 3547 Å

A. Experiment

Five of the materials studied at 5321 Å were studied at 3547 Å. NaCl was eliminated from the uv study because of surface scattering from polishing scratches.

The experimental arrangement used at 3547 Å is identical to that shown in Fig. 3, up to the CsH_2AsO_4 cell (HG2). In the uv experiment, a beam splitter (just after HG2) and filtered detector P4 monitored the second-harmonic conversion efficiency. The 1.064-μm and 5321-Å orthogonally polarized pulses then traveled collinearly through a final KH_2PO_4 frequency-summing crystal. This crystal was angle tuned for the phase-matched generation of third-harmonic 3547-Å light. Unfortunately, no material is available with the proper temperature behavior of refractive indices (ordinary and extraordinary) to allow temperature-tuned, 90° phase-matched frequency summing at these two input wavelengths. Spatial separation of the three output pulses was then performed by a quartz prism. Next a quartz beam splitter directed a sample of the 3547-Å pulse to a self-scanning Si photodiode array which enabled the pulse spatial profile of each shot to be displayed on an oscilloscope. The energy content of the uv pulse was monitored by another quartz beam splitter and a filtered, calibrated photodiode. The calibrated uv pulse then passed into the light-shielded breakdown chamber and was tightly focused by a quartz lens (L) into the dielectric sample (S) under investigation. Owing to the typical magnitude of the breakdown input power relative to the self-focusing critical power, data in this experiment were taken only with our shortest focal length (0.5 in.) lens.

It is clear[1] that three pulse parameters—the total pulse energy $\mathcal{E}$, the temporal half-duration τ, and the spatial profile radius ρ (or better the focal radius w)—must be carefully measured to allow the accurate determination of the electric field distribution of the optical pulse. The sufficiency of these three parameters is based on the assumption that the pulse spatial and temporal functional form is unchanging. We will next discuss the degree to which the characteristics of the 3547-Å pulses allowed us to determine their field distribution.

The third-harmonic pulse energy ($\mathcal{E}_{TH}$) measurement is straightforward, as it was in the 5321-Å and earlier 1.064-μm experiments. The 3547-Å detector was calibrated again with two Eppley Laboratory thermopiles, which were themselves calibrated with National Bureau of Standards spectral sources. Again, the detector area is large enough and the detector-oscilloscope response time is long enough that true spatial and temporal integration is performed over the pulse waveform by the detector. Our calibration method yields pulse energy measurements with an estimated accuracy of better than ±10%.

The temporal waveform of the 3547-Å pulse should be closely Gaussian for small conversion efficiencies in both the doubling and mixing crystals. In that case, the average duration of the uv pulse will be $1/\sqrt{3}$ of the 30-psec 1.064-μm parent pulse average duration (or 17 psec). This $1/\sqrt{3}$ degree of pulse shortening has been roughly confirmed experimentally with streak camera photography.[46] As the conversion efficiency increases, preferential saturation of the doubling and mixing processes at the temporal peak region of the pulse results in an effective lengthening of the duration. The saturation results simultaneously in an effective broadening[45] of the pulse area as the pulse becomes more square in profile. Fortunately, our experimental procedure—specifically the τA technique[40]—allows us to incorporate these broadening factors into our data analysis. In the low conversion regime, it is easily shown that the ratio $(\mathcal{E}_f^3/\mathcal{E}_{TH})^{1/2}$ of the fundamental (f) and third-harmonic (TH) pulse energies is directly proportional to the third-harmonic pulse area A and half duration τ and is independent of the pulse intensity. For data in the low conversion regime, we may normalize the individual pulse $(\mathcal{E}_f^3/\mathcal{E}_{TH})^{1/2}$ signals to a product of a half duration τ of 17 psec and the actual pulse area as measured with the photodiode array. Then for the remaining data points in the higher-power range, the signals will become progressively larger and will properly take into account the broadening of the duration and area. Direct picosecond-resolution streak camera photography is the only technique available which would permit a more accurate correction for this temporal broadening.

We have discussed the energy and pulse-duration measurements and the minor saturation broadening of the pulse area $\pi\rho^2$. It remains to consider the distortions in the pulse spatial profile which are due to walk-off and self-focusing in the KH_2PO_4 mixing crystal. Figure 8 illustrates the typical spatial distribution of energy that we obtained in a 3547-Å pulse. Walk-off[47] is the term which describes the decrease in overlap, proportional to the distance traveled inside the nonlinear crystal, between the nonlinear polarization wave and the generated light wave. Walk-off is caused by crystal birefringence, and it results in a cylindrically asymmetric, distorted spatial waveform for the 3547-Å pulse. The poor spatial profile exhibited in Fig. 8(a) is the result in the plane

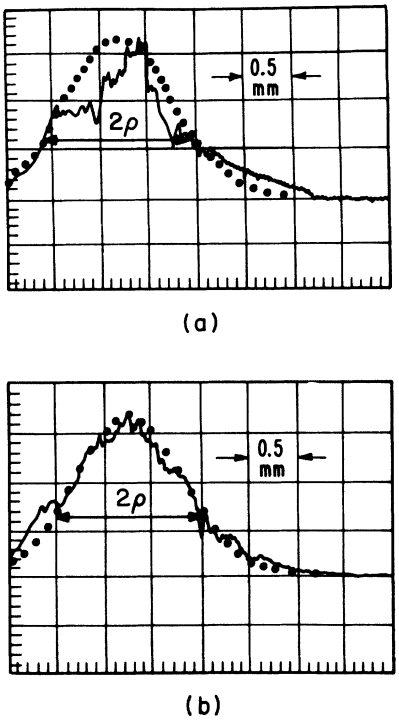

FIG. 8. Oscillogram tracings (solid curves) of the spatial distribution of the 3547-Å light pulse. Figures (a) and (b) are taken in the planes of most and least influence from walk-off, respectively. The dotted curves illustrate the fitting of a Gaussian function to the actual profiles. The profile radius ρ is used to compute the area of the pulse in the focal plane of a lens.

most severely affected. Figure 8(b) shows the distortion which occurs in the plane normal to that of Fig. 8(a). One observes in these photographs the departure of our spatial profile from a Gaussian form.

Nevertheless, the input area of the uv pulse of Fig. 8 must be estimated by fitting to it a Gaussian curve, as shown there. The input profile radius ρ (0.81 mm), obtained from the dotted Gaussian curves, yields a focal area A ($=\pi w^2$) of 5.6 μm^2. If the laser profiles conformed to the dotted Gaussian curves perfectly, the uncertainty in A would be less than ±20%, as was the case in our experiments at 1.064 μm. The actual fit of the profile in Fig. 8(b) is acceptable, but because of the modulation evident in Fig. 8(a), the fit there is poor and leads to additional uncertainty in the focal plane area. Since the lens essentially performs a Fourier transformation, the abrupt transverse intensity variations (high spatial-frequency modulation) of the input pulse result in a deconcentration of the energy distribution in the focal plane which is not taken into account by the Gaussian beam propagation equations used above to arrive at the area of 5.6 μm^2. Rough estimation indicates that the actual effective area might be as much as a factor two larger than the 5.6 μm^2 value obtained by Gaussian approximation.

If the laser spatial profile were constant from pulse to pulse over the period of time necessary for an experiment to be performed, the scanning aperture technique[1] could be used to measure the effective area in the focal plane. That avenue of relief was blocked in this experiment by the last distortions which must be mentioned and which are both time and power dependent. Over a period of a few (~3–5) minutes, minute movements in the optical table resulted in variations in the KH_2PO_4 phase-matching angle, and the large-scale fringe structure in Fig. 8 wandered correspondingly. And at high-power levels self-focusing of the 3547-Å pulse in the KH_2PO_4 crystal and in the subsequent quartz elements significantly enhances the noise structure produced by the phase-matching conditions. Spatial spot enhancement by self-focusing was present in the breakdown tests of all materials except CaF_2. This effect results in different, uncalculable reductions in the effective focal area for materials which undergo breakdown at different power levels. The influence of this effect is in opposite direction to the enlargement of the focal area, mentioned earlier, caused by the Fourier transform of high spatial-frequency components on the input pulse. Therefore the true effective focal area for CaF_2 is probably nearer the 11.2-μm^2 estimation than the 5.6-μm^2 value, but for materials with increasingly higher threshold power, the probable effective area is reduced to values closer to 5.6 μm^2 and perhaps less by hot spot enhancement. This material dependent effective area makes difficult the extraction and substantiation of even relative breakdown thresholds from this 3547-Å experiment.

The procedure for this experiment is identical to that of the 5321-Å experiment as related in Sec. III A2.

B. Results

The data from the 3547-Å experiment are listed in Table IV. The five tested materials are KH_2PO_4, fused SiO_2, CaF_2, NaF, and LiF. These five materials were studied at the two previous wavelengths of 1.064 μm and 5321 Å. The linear refractive indices n_0 at 3547 Å are listed in column 2. Columns 3 and 4 tabulate the "paraxial" critical power P_1 and the "catastrophic" critical power P_2, calculated using the nonlinear refractive index (n_2) values listed in Table I. Because of the λ^2 dependence of P_1 and P_2, the 3547-Å critical power values in Table IV are smaller than

TABLE IV. 3547-Å breakdown data.

Material	n_0	P_1 (kW)	P_2 (kW)	P (kW)	P/P_1	P/P_2	$\phi(P)$	E_B^{uv} (MV/cm)	Δ_2 [a]
KH_2PO_4	1.5316	119	439	242	2.03	0.55	2.5–3.7	35–77	1.5–3.3
SiO_2	1.4762	125	462	170	1.36	0.37	2.0–3.0	25–49	1.3–2.6
CaF_2	1.4463	105	390	73	0.69	0.19	1.0–1.5	18–33	0.7–1.3
NaF	1.3359	126	465	271	2.15	0.58	2.5–3.7	40–99	2.1–5.1
LiF	1.4024	129	477	245	1.90	0.51	2.5–3.7	35–70	1.3–2.6

[a]The quantity Δ_2 is defined as E_B^{uv} (17 psec)/$E_B^{\mathcal{E}}$ (21 psec).

the corresponding entries in Table I by a factor of $\frac{9}{4}$. In column 5 the measured values of the pulse input power at the breakdown threshold are listed, and columns 6 and 7 tabulate the fractional quantities P/P_1 and P/P_2.

As discussed in Sec. II, the breakdown threshold electric field E_B may be obtained from the threshold power P by the use of Eq. (6). The obstacles of the interpretation and extraction of a breakdown threshold electric field from the data of Table IV are twofold. One of them has already been mentioned and it is the substantially non-Gaussian and unavoidably poor spatial character of the 3547-Å pulse due to the details of the final frequency mixing process and self-focusing. The specific result of the propagation of that distortion into the focal plane is that the intensity distribution there is irregular with an effective area A known only to within a factor 2. The probable effective area varies with input power, as well.

The other obstacle is the magnitude of the breakdown threshold power P relative to P_1 and P_2. As the entries in columns 6 and 7 show, the P values fit neither of the two limits mentioned following Eq. (6) in Sec. II. The CaF_2 input power more closely fits the $P \ll P_1$ limit, while the other input powers more closely approach the $P \lesssim P_2$ limit. It is therefore necessary to consider different ranges of the $\phi(P)$ function for the different materials, in order to deduce realistic upper and lower bounds for E_B from Eq. (6). Column 8 of Table IV lists the considered ranges of $\phi(P)$. In comparison to the large uncertainties introduced by the area A (5.6–11.2 μm^2) and by $\phi(P)$ in Eq. (6), the small (± 10%) uncertainty in the input power P is immaterial and therefore neglected.

The next to the last column of Table IV lists the 3547-Å breakdown threshold [E_B^{uv}(17 psec)] results obtained in this experiment. The stated range in E_B^{uv} results from the uncertainties in A and $\phi(P)$. The lower and upper limits of E_B^{uv} for each material were obtained with the use of the upper and lower, respectively, limits of A and $\phi(P)$. The range of E_B^{uv} for a given material in column 9 constitutes an uncertainty of ~ ± 35% about the average of the upper and lower limits. The reason the data were not displayed in that manner is that the power (and thus material) dependent hot spot behavior points to different probable location of the true threshold within that ± 35% range for the different materials. For example, for CaF_2 the true threshold is closer to 18 than 33 MV/cm, due to the small P/P_1 factor and the resulting absence of hot-spot enhancement. But for LiF, the true E_B^{uv} may be nearer 70 than 35 MV/cm.

In order to find whether interesting frequency-dependent behavior is resolvable in this data, in Fig. 9 we plot the range of the ratio E_B^{uv} (17 psec)/$E_B^{\mathcal{E}}$ (21 psec), denoted Δ_2, versus material band gap. The 5321-Å thresholds ($E_B^{\mathcal{E}}$) are taken from Table II. Here we ignore the common effect of the small pulse duration difference (nominally 17 psec at 3547 Å vs 21 psec at 5321 Å) on the threshold ratio.

The relative and absolute positions of the Δ_2 data bars for CaF_2 and LiF seem reasonable, in view of the similar data of Fig. 7. We also observe an absolute increase in the NaF threshold, as expected. Yet the reason for relative mag-

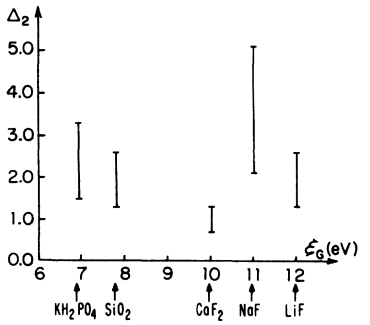

FIG. 9. Illustration of the band gap ($\mathcal{E}_G$) dependent behavior of the observed threshold ratio Δ_2, defined as E_B^{uv} (17 psec)/$E_B^{\mathcal{E}}$ (21 psec). The origins of the uncertainty in the data are discussed in the text.

nitudes of the NaF and LiF Δ_2 values is not known, unless it is the simple manifestation of the large experimental uncertainties. The observation that the Δ_2 values for KH_2PO_4 and SiO_2 in Fig. 9 are as large or larger than that for LiF can be explained, however. In Sec. III B the interpretation was advanced for the data of Fig. 7 that the marginal onset of three-photon absorption (3PA) lowered the KH_2PO_4 threshold at 5321 Å relative to that at 1.064 μm. If we apply that observation to the present 3547-Å experiment, we conclude that the 3PA might serve to lower the thresholds for materials with band gap less than 10.5 eV. CaF_2 has a band gap of 10 eV and indeed in Fig. 9 one observes that the Δ_2 bar for CaF_2 allows the possibility that the 3547-Å threshold is less than the 5321-Å threshold. For SiO_2, 3PA would be considerably stronger due to its band gap of about 8.0 eV. 3PA is less nonlinear in the electric field than is avalanche ionization, and may occur over a correspondingly less localized region about the focal point. It is expected that 3PA caused beam depletion along the focal axis in front of the focal point in the SiO_2 sample, thereby reducing the highest field attainable (at the focal point) in the sample. Because the avalanche ionization rate is highly nonlinear,[1] the conceivable net result of this pulse depletion by 3PA (even though it produces free carriers) is an apparent increase in the 3547-Å breakdown threshold over the longer-wavelength thresholds. Therefore the observation of a Δ_2 value exceeding unity for SiO_2 is an indication not of true threshold behavior but merely of pulse depletion, in the sense that 5321- and 3547-Å threshold measurements performed on the surface of SiO_2 should yield a Δ_2 value less than unity. A similar explanation may be advanced for the even larger Δ_2 values observed for KH_2PO_4. For that material, *two*-photon absorption (2PA) is energetically allowed at 3547 Å, and beam depletion before the focal point would be more severe. Unfortunately it is not presently possible to account for the multiphoton absorption depletion by calculation, because the 3547-Å coefficients for 3PA in SiO_2 or 2PA in KH_2PO_4 are not known.

V. DISCUSSION

In Sec. III B1 and IV B we interpreted the measured, frequency-dependent threshold changes in terms of the two-component picture of laser-induced breakdown which is schematized in Fig. 1. The interesting behavior there is provided by competition between the frequency trends of avalanche ionization and multiphoton absorption. One would like to be able to directly compare the experimental data of Figs. 7 and 9 with existing theoretical predictions. At present, however none have been presented for our experimental conditions of wavelength and pulse duration. This situation is due to the unavailability of experimental multiphoton absorption coefficients at 1.064 μm and 5321 Å. This absence is unfortunate because the only available avalanche ionization rate data for laser-induced breakdown is for 1.064-μm wavelength in alkali-halides.[1,48,49]

Multiphoton ionization coefficients have been measured (by photoconductivity detection) at 6943 and 3472 Å in NaCl, KCl, and KI, however, by Catalano *et al.*[50] and Dneprovskii *et al.*[51] Braünlich *et al.*[21] have used that data, along with the 1.064-μm avalanche ionization rate data (neglecting its frequency dispersion) to investigate numerically the influence of multiphoton absorption on breakdown in NaCl at 6943 and 3472 Å (30-nsec full width at half maximum pulse duration). They calculated, as a function of light intensity, the conduction-electron density generated by pure avalanche ionization, by avalanche ionization with five-photon interband absorption, and by avalanche with five-photon absorption and an F-center population. Their results showed that multiphoton absorption, both interband and via F-center levels, is more efficient at producing initial electrons at low field strengths than is avalanche ionization. They also showed that the avalanche ionization efficiency dominates the plasma generation for electric field strengths over about 1 MV/cm, regardless of the presence of the other multiphoton mechanisms. Our morphological data, at 1.064 μm and 5321 Å (Fig. 5),[3] indicate that the last statement is indeed true. At both of those wavelengths we observed the same morphology, even in KH_2PO_4 at 5321 Å where three-photon transitions are possible. At both wavelengths the morphology consisted of spatially distinct plasma sites separated irregularly by short (~ 1 μm) undamaged spaces. If strong multiphoton absorption were dominant in the breakdown process, one would expect to see, not spatially distinct plasma vestiges, but spatially *continuous* evidence of damage along the focal axis even at breakdown threshold. As Fig. 5 demonstrates, that is not the case. At 5321 Å, in materials with $\mathcal{E}_G > 7$eV and with pulses of picosecond duration, the character of intrinsic picosecond laser-induced breakdown is still dominated by the familiar avalanche ionization mechanism.

At 3547 Å, however, for materials with band gap $\lesssim 10$ eV, multiphoton absorption effects are manifest in the breakdown data. Although we were not able to study NaCl at 3547 Å, the calculations of Bräunlich *et al.*[21] for NaCl at 3472 Å may be examined in light of our 3547-Å data for other ma-

terials. The data of Fig. 9 indicate that the 3547-Å threshold for NaCl (8.7-eV band gap) would be lowered by 3PA transition, as predicted by the calculations in Ref. 21. The data also indicate that the depletion effect in a bulk experiment would complicate the extraction of a precise measure of the reduction, however.

The indications of strong multiphoton absorption in KH_2PO_4 and SiO_2 at 3547 Å suggest that if the breakdown experiment had been conducted on the sample surface rather than in the bulk, large decreases in the thresholds might have been observed at 3547 Å. The study of breakdown on surfaces would alleviate two difficulties which complicated the study described in this chapter—self-focusing in the sample and multiphoton absorption pulse depletion in the sample. Because of the wavelength dependence of these two factors, surface breakdown study will be increasingly attractive for wavelengths below 3547 Å. The use of 2661-Å fourth-harmonic light, generated entirely with 90° phase-matched materials [cesium dihydrogen arsenate (CDA) and ammonium dihydrogen phosphate (ADP)], for such a study would remove walk-off distortion, as well. The benefits of surface breakdown study in the ultraviolet spectral region will be offset somewhat by other well-known problems[52] associated with surface breakdown. Those problems originate with surface impurities and imperfections. Because they generally introduce the possibility for errors of typically a factor 2 in threshold electric field measurements, the surface quality problems will require serious attention and solution if accurate and reproducible thresholds are to be obtained.

Another recent theoretical analysis has been made by Sparks.[4,25] He included electron-photon-phonon transitions as a new mechanism for sustaining an avalanche, and he also included multiphoton absorption for initial electron generation. His theoretical threshold values for 10.6-μm, 1.06-μm, and 6943-Å laser-induced breakdown fall within the uncertainty limits of the experimental values, a measure of progress, indeed, in theoretical threshold calculations. His calculations also predicted a decrease in the NaCl threshold to be observed for wavelengths shorter than about 1.0 μm for nanosecond pulse (Fig. 3 of Ref. 4). In particular, a decrease of ~50% was forecast between 1.064 μm and 5321 Å. The picosecond data presented here do not follow that prediction, but suggest that a threshold decrease may be expected in NaCl only for wavelengths shorter than about $3hc/\mathcal{E}_G \simeq 4300$ Å. Several other points raised in Refs. 4 and 25 merit discussion. It was stated in these papers that the difference between early dc thresholds and those measured by Yablonovitch[9] was attributed to avalanche ionization frequency dependence, as embodied in Eq. (1). That assertion is incorrect. Yablonovitch[9] warned against such assignment of the systematic difference that he found, and indicated that the more probable origin of that factor concerns details of the dc experiments. Others[19] have restated that point. Concerning the avalanche ionization frequency dependence as given by Eq. (1), both the present work and an earlier experiment[11] indicate that τ_c is of the order 2×10^{-16} sec, whereas the calculations of Sparks[25] predict that τ_c should be larger roughly by the factor 10. A final point concerns the initial density of electrons that may serve to launch an avalanche. It has been argued[4] that because of insulator electrical conducitivity and photoconductivity values, initial electron densities should be less than ~10^4 cm^{-3} and that densities as large as 10^{10} cm^{-3} are unreasonable. Yet direct experimental evidence of such large densities has been found in picosecond laser-induced breakdown morphology.[3] The resolution of this point lies in the fact that photoconductivity measurements usually involve light intensities too weak to permit the ionization of color center traps by multiphoton absorption, and photon energy too small to allow single-photon defect ionization. Color center densities as low as 10^{11} cm^{-3} are difficult to detect by linear absorption spectrophotometry. It is therefore possible to have a clear NaCl sample which satisfies the insulator criterion (dc conductivity $\sigma \lesssim 10^{-20}$ Ω^{-1} cm^{-1}), yet simultaneously possesses 10^{11}-cm^{-3} F centers which may be ionized by 1.064-μm two-photon absorption to produce breakdown morphology as observed in Ref. 3.

VI. SUMMARY

The study of picosecond laser-induced breakdown has been quantitatively extended to 5321 Å. Laser pulses at 5321 Å having sufficiently reproducible and Gaussian spatial intensity distribution were produced by the frequency doubling of 1.064 μm, YAlG:Nd laser pulses in a 90° phase-matched crystal. Except for a specific uncertainty regarding spatial distortion by self-focusing, which could be eliminated with numerical study, the thresholds for dielectric breakdown at 5321 Å were determined to an accuracy of ±15%. These thresholds were compared to 1.064-μm thresholds, adjusted for pulse duration dependence, from a previous study. The comparison showed that for a material allowing interband three-photon absorption to assist the avalanche process at 5321 Å, dielectric breakdown at 5321 Å requires a lower electric field than at 1.064 μm. For other materials with optical band gap larger than three

5321-Å photons, the influence of multiphoton transitions is weaker, and stronger fields were required to induce breakdown at 5321 Å than at 1.064 μm. This measured frequency-dependent increase varied smoothly with material band gap from almost zero up to about 44% for LiF.

We have seen that the 3547-Å data of Fig. 9 is both explicable and reasonable in light of the earlier data obtained at the wavelengths of 1.064 μm and 5321 Å and displayed in Fig. 7. Although the uncertainties introduced by pulse distortion did not allow the determination of precise breakdown thresholds at 3547 Å, the frequency-dependent behavior observed first at 5321 Å was verified and extended qualitatively. Larger thresholds were found at 3547 Å, than at 5321 Å or 1.064 μm, for materials which do not permit two- or three-photon interband absorption to occur at 3547 Å. The data for one material, CaF_2, which supports weak three-photon absorption at 3547 Å, allowed the possibility of a decrease in the 3547-Å threshold, compared to its 5321-Å threshold. Such threshold behavior at 3547 Å in CaF_2 corresponds energetically to that found in KH_2PO_4 as the light frequency was doubled to 5321 Å in the prior investigation. At 3547 Å, for materials (KH_2PO_4 and SiO_2) with optical band gap smaller than that of CaF_2, an increase in the threshold input power was also observed. However, those increases were interpretable as arising from depletion of the laser pulse, by strong two- or three-photon absorption, as it passed through the sample toward the focal region.

The main conclusion of this work is that the breakdown threshold does increase with light frequency, as predicted[19] by the avalanche ionization model, up to the frequency where three-photon absorption may take place. Beyond that frequency, the assistance of the essentially instantaneous multiphoton absorption transitions is sufficient to reverse the avalanche ionization frequency trend, with the net result that the breakdown threshold is reduced. These observations provide experimental verification for the behavior of the breakdown processes through the transition from the low-frequency ($\hbar\omega$ much smaller than the band gap) to the high-frequency ($\hbar\omega$ of the order of the band gap) regime.

A report of this work was presented at the IX International Conference on Quantum Electronics, Amsterdam, The Netherlands, June, 1076. More recently we learned that Newnam and Gill[53] at Los Alamos Scientific Laboratory investigated the damage resistance of refractory oxide (band-gap range of 3.6–7.8 eV) quarterwave thick films deposited onto silica substrates. Their measurements were carried out at 1.064 μm, 5321 Å, and 3547 Å, and they also have reported threshold increases at 5321 Å and decreases at 3547 Å.

ACKNOWLEDGMENTS

We thank Professor J. H. Marburger of the University of Southern California for a helpful discussion concerning self-focusing. Dedicated sample preparation by S. Maurici is once again greatly appreciated.

---

*Research supported in part by the National Aeronautics and Space Administration, by the Joint Services Electronics Program, and by the Advanced Research Projects Agency.

†Present address: Lawrence Livermore Laboratory, University of California, Livermore, Calif. 94550.

‡Present address: General Motors Research Laboratory, Warren, Mich. 48090.

[1]W. Lee Smith, J. H. Bechtel, and N. Bloembergen, Phys. Rev. B 12, 706 (1975).

[2]W. Lee Smith and J. H. Bechtel, Appl. Phys. Lett. 28, 606 (1976).

[3]W. Lee Smith, J. H. Bechtel, and N. Bloembergen, Opt. Commun. 18, 592 (1976).

[4]M. Sparks, *Laser Induced Damage in Optical Materials: 1975*, Natl. Bur. Stds. Special Pub. No. 435 (U.S. GPO, Washington, D. C., 1976), p. 331.

[5]A. Van Marum, Ann. Phys. (Leipz.) 1, 68 (1799).

[6]A. von Hippel, Z. Phys. 67, 707 (1931); J. Appl. Phys. 8, 815 (1937); Phys. Rev. 54, 1096 (1938).

[7]H. Fröhlich, Proc. R. Soc. Lond. 160, 230 (1937); 188, 521; 188, 532 (1947), and references therein.

[8]F. Seitz, Phys. Rev. 76, 1376 (1949); see also H. Callen, *ibid.* 76, 1394 (1949).

[9]E. Yablonovitch, Appl. Phys. Lett. 19, 495 (1971).

[10]D. Fradin, E. Yablonovitch, and M. Bass, Appl. Opt. 12, 700 (1973).

[11]D. Fradin and M. Bass, Appl. Phys. Lett. 22, 206 (1973).

[12]M. Bass and H. H. Barrett, Appl. Opt. 12, 690 (1973).

[13]G. M.-Zverev, T. N. Mikhailova, V. A. Pashkov, and N. M. Solov'eva, Zh. Eksp. Teor. Fiz. 53, 1849 (1967) [Sov. Phys.-JETP 26, 1053 (1968)].

[14]G. M. Zverev, E. A. Levchuk, and E. K. Maldutis, Zh. Eksp. Teor. Fiz. 57, 730 (1969) [Sov. Phys.-JETP 30, 400 (1970)].

[15]R. Yu. Orlov, I.B. Skidan, and L. S. Telegin, Zh. Eksp. Teor. Fiz. 61, 784 (1971) [Sov. Phys.-JETP 34, 418 (1972)].

[16]S. A. Belozerov, G. M. Zverev, V. S. Naumov, and V. A. Pashkov, Zh. Eksp. Teor. Fiz. 63, 294 (1972) [Sov. Phys.-JETP 35, 158 (1972)].

[17]V. A. Gridin, A. N. Petrovskii, and S. L. Pestmal, Kvant. Electron. 1, 2278 (1974) [Sov. J. Quantum Electron. 4, 1270 (1975)].

[18]V. A. Gridin, V. A. Krotov, and A. N. Petrovskii,

Kvant. Electron. 3, 311 (1976) [Sov. J. Quantum Electron. 6, 163 (1976)].
[19]N. Bloembergen, IEEE J. Quantum Electron. QE-10, 375 (1974).
[20]L. V. Keldysh, Zh. Eksp. Teor. Fiz. 47, 1945 (1964) [Sov. Phys.-JETP 20, 1307 (1965)]; see also S. S. Mitra, L. M. Narducci, R. A. Shatas, Y. F. Tsay, and A. Vaidyanathan, Appl. Opt. 14, 3038 (1975). Our calculations follow those of Mitra *et al.*
[21]P. Braünlich, A. Schmid, and P. Kelly, Appl. Phys. Lett. 26, 150 (1975).
[22]P. Kelly, P. Braünlich, and A. Schmid, Appl. Phys. Lett. 26, 223 (1975).
[23]N. L. Boling, P. Braünlich, A. Schmid, and P. Kelly, Appl. Phys. Lett. 27, 191 (1975).
[24]L. H. Holway and D. Fradin, J. Appl. Phys. 46, 279 (1975).
[25]M. Sparks and C. J. Duthler (Fifth Technical Report on Contract No. DAHC 15-73-C-0127, Xonics Corp., Van Nuys, Calif. 91406, 1975) (unpublished).
[26]See p. xxvii of Ref. 4 for a full listing of Natl. Bur. Stds. Special Publications of Proceedings of Conferences on Laser-Induced Damage in Optical Materials, 1969–1975.
[27]J. J. O'Dwyer, *The Theory of Electrical Conduction and Breakdown in Solids and Dielectrics* (Clarendon, Oxford, 1973).
[28]J. H. Marburger, in *Progress in Quantum Electronics*, edited by J. H. Sanders and S. Stenholm (Pergamon, Oxford, 1975), Vol. 4, Part 1, and references therein.
[29]V. I. Talanov, Zh. Eksp. Teor. Fiz. 2, 218 (1965) [Sov. Phys.-JETP Lett. 2, 138 (1965)].
[30]P. L. Kelley, Phys. Rev. Lett. 15, 1005 (1965).
[31]G. M. Zverev and V. A. Pashkov, Zh. Eksp. Teor. Fiz. 57, 1128 (1969) [Sov. Phys.-JETP 30, 616 (1970)].
[32]D. Fradin, IEEE J. Quantum Electron. QE-9, 954 (1973). Note that Eq. (2) in this reference should read $I_d = I_0(1-P/P_{cr})^{-1}$.
[33]A. Feldman, D. Horowitz, and R. M. Waxler, IEEE J. Quantum Electron. QE-9, 1054 (1973).
[34]P. D. Maker and R. W. Terhune, Phys. Rev. 137, A801 (1965).
[35]A. Owyoung, IEEE J. Quantum Electron. QE-9, 1064 (1973).
[36]M. D. Levenson, IEEE J. Quantum Electron. QE-10, 110 (1974); M. D. Levenson and N. Bloembergen, Phys. Rev. B 10, 4447 (1974).
[37]E. S. Bliss, D. R. Speck, and W. W. Simmons, Appl. Phys. Lett. 25, 728 (1974).
[38]M. J. Moran, C-Y. She, and R. L. Carman, IEEE J. Quantum Electron. QE-11, 259 (1975).
[39]D. Milam and M. J. Weber, J. Appl. Phys. 47, 2497 (1976).
[40]W. Lee Smith and J. H. Bechtel, J. Appl. Phys. 47, 1065 (1976); J. H. Bechtel and W. Lee Smith, Phys. Lett. A 55, 203 (1975).
[41]K. Kato, IEEE J. Quantum Electron. QE-10, 616 (1974); see also the discussion of 90° phase matching in F. Zernike and J. E. Midwinger, *Applied Nonlinear Optics* (J. Wiley, New York, 1973), Chap. 3.
[42]W. Lee Smith, J. H. Bechtel, and N. Bloembergen, in *Laser-Induced Damage in Optical Materials*: 1975, Natl. Bur. Stds. Special Pub. No. 435 (U.S. GPO, Washington, D. C., 1976), p. 321.
[43]W. J. Deshotels, J. Opt. Soc. Am. 50, 865 (1960).
[44]W. Lee Smith, J. H. Bechtel, and N. Bloembergen (unpublished).
[45]D. R. White, E. L. Dawes, and J. H. Marburger, IEEE J. Quantum Electron. QE-6, 793 (1970).
[46]D. T Attwood, E. L. Pierce, and L. W. Coleman, Opt. Comm. 15, 10 (1975).
[47]The phenomenon of walk-off was originally termed the "aperture effect" by early authors: D. A. Kleinman, Phys. Rev. 128, 1761 (1962). See also G. D. Boyd, A. Ashkin, J. M. Dziedzic, and D. A. Kleinman, *ibid.* 137, A1305 (1965).
[48]E. Yablonovitch and N. Bloembergen, Phys. Rev. Lett. 29, 907 (1972).
[49]D. W. Fradin, N. Bloembergen, and J. P. Lettelier, Appl. Phys. Lett. 22, 635 (1973).
[50]I. M. Catalano, A. Cingolani, and A. N. Minafra, Phys. Rev. B 5, 1629 (1972).
[51]V. S. Dreprovskii, D. N. Klyshko, and A. N. Penin, Zh. Eksp. Teor. Fiz. 3, 385 (1966) [Sov. Phys.-JETP Lett. 3, 251 (1966)].
[52]N. Bloembergen, Appl. Opt. 12, 661 (1973).
[53]B. E. Newnam and D. H. Gill, presented at and to be published in the Proceedings of the 8th Annual Symposium on Optical Materials for High Power Lasers, Boulder, Colo., July 1976 (unpublished). (The reader should note while interpreting that and the present paper that no normalization factor to account for pulse-duration dependence of the threshold was applied to the data of Newnam and Gill, as they state.)

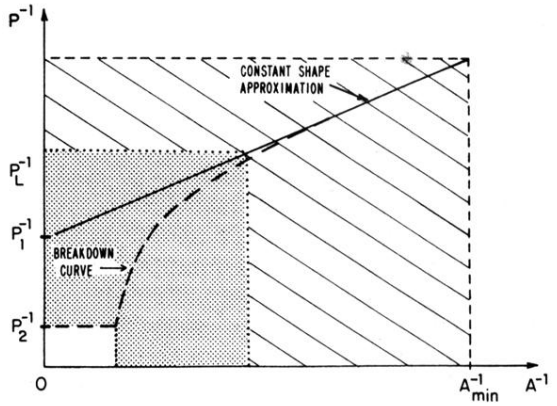

FIG. 2. Illustrations of the slope-intercept breakdown construction, as given by Eqs. (5) and (6), wherein one plots for a given lens the reciprocal pulse input power (P^{-1}) versus reciprocal focal area (A^{-1}). The dashed curve is defined by the breakdown and self-focusing properties of the material, and the solid line is from the constant shape approximation. P_1 and P_2 are the "paraxial" and the "catastrophic" critical powers, respectively. See Sec. II for a discussion of the two curves. A_{min} is the minimum focal area obtainable with a given wavelength.

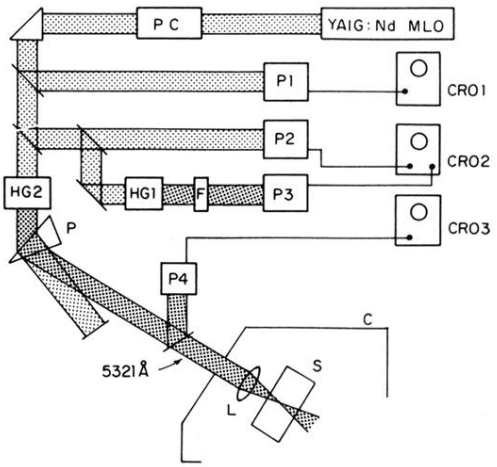

FIG. 3. Schematic diagram of the experimental apparatus. Notation: MLO, mode-locked YAlG:Nd laser oscillator; PC, Pockels cell single pulse selector; P1-P4, photodiode detectors; CRO1, Tektronix 519 oscilloscope; CRO 2-3, Tektronix 555 oscilloscopes; HG1, KH_2PO_4 5321-Å generation cell; HG2, CsH_2AsO_4 temperature-tuned 5321-Å generation cell; F, green-pass filter; P, dispersing prism; C, curtain; L, lens; S, material sample.

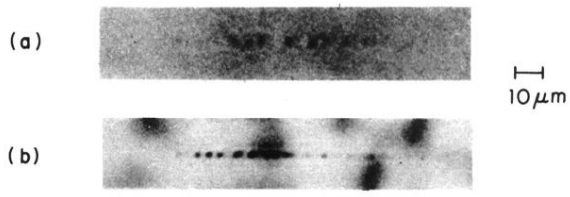

FIG. 5. Breakdown morphology in (a) KH_2PO_4 and (b) LiF, induced by 5321-Å picosecond laser pulses focused to an e^{-1} rms electric field focal radius of 3.1 μm. The scale markers denote a distance of 10 μm, and the pulses were incident from the left-hand side. The maximum rms electric field reached at the focal point for photographs (a) and (b) were 14 and 40% above the respective thresholds for the two materials. The mottled background appearance in (b) is immaterial.